TECHNICAL ARTICLE

Optimizing surface properties in pure titanium for dental implants: a crystallographic analysis of sandblasting and acid-etching techniques

Krisna Adhitya,[1,a] Tika Mustika,[1] Maykel Manawan,[1,2] Ika Maria Ulfah,[1] Razie Hanafi,[1] Iwan Setyadi,[1] Suryadi,[1] Arif Hidayat,[1] Mirza Wibisono,[1] Joni Sah,[1] Giri Wahyu Alam,[1] Muslim Efendi Harahap,[1] Hadi Prianto Sulaikan,[1] Nandang Suhendra,[1] and I Nyoman Jujur[1]

[1]*Advanced Material Research Center, National Research and Innovation Agency (Indonesia), B.J. Habibie Building 15th–24th Floor, Jl. M.H. Thamrin No. 8, Central Jakarta 10340, Indonesia*

[2]*Indonesia Defense University, Kawasan Indonesia Peace and Security Center (IPSC), West Java 16810, Indonesia*

(Received 24 August 2023; accepted 13 June 2024)

Surface roughness is a critical factor affecting the performance of dental implants. One approach to influence this is through sandblasted, large grit, acid-etched (SLA) modification on pure titanium implant surfaces. In this study, SLA was performed on grade IV pure titanium. Sandblasting was conducted at distances of 2, 4, and 6 cm. Subsequently, the samples were etched with a mixed acid solution of HCl, H_2SO_4, and H_2O for 0, 30, and 60 min. Surface roughness and X-ray diffraction (XRD) characterizations were conducted on the samples. The results revealed that surface roughness increased but was not too significant as the sandblasting distance decreased. Longer etching durations for sandblasted with acid-etched samples led to reduced surface roughness (*Sa* and *Sz*). It was found that a 60 min-etched sample resulted in optimal *Sa*, *Sz*, and *Ssk* values, i.e., 1.19 μm, 13.76 μm, and −0.60, respectively. The XRD texture was significantly influenced by sandblasting, with compressive residual stress increasing as the sandblasting distance decreased. Normal stress causes hill formations at shorter sandblasting distances. For etched samples, the residual stress decreased with longer etching durations. Normal stress-decreasing trend aligns with the initial reduction in hill and valley within the samples and subsequent hill enhancement at extended etching duration.

[doi:10.1017/S0885715624000320]

Keywords: dental implant, pure titanium, SLA, surface roughness, texture, residual stress

I. INTRODUCTION

Pure titanium has been widely used as raw materials for bone and dental implants (Carlsson et al., 1986; Semlitsch, 1987; Buser et al., 1991; Donley and Gillette, 1991; Klokkevold et al., 1997). Titanium possesses excellent biocompatibility, high mechanical strength, and exceptional corrosion resistance. Surface roughness represents a significant parameter for enhancing the performance of titanium-based dental implants. Surface modification is a viable approach to improving the roughness of titanium implants, and a commonly employed technique for this purpose is the combination of sandblasting and acid-etching, known as SLA (Sandblasted, Large grit, Acid-etched). This subtractive modification method offers the advantage of creating a highly rough surface with nanometer-sized pores, facilitating improved contact between the implant and the bone/tooth host. Based on a Straumann AG patent, three 3D roughness parameters (*Sa*, *Sz*, and *Ssk*) with values of 0.9 to 1.5 μm, 6.0 to 12.0 μm, and −0.3 to 0.5, respectively, are recommended to optimize the performance of titanium-based implants (Wennerberg and Albrektsson, 2009; Berner, 2016; Medvedev et al., 2016). *Sa* is the arithmetic mean height of the surface (μm), *Sz* is the maximum peak-to-valley distance (μm), and *Ssk* is the symmetry of peaks and valleys distribution on the surface (unitless) (Monetta and Bellucci, 2012). Furthermore, the SLA technique is known to induce compressive residual stress on the modified implant surface, which plays a crucial role in enhancing the implant's fatigue resistance and the contact between the surface of bone cells and the titanium implant.

An abundance of literature discusses the effects of SLA modification and its variations on the surface of pure titanium implants. Until now, there has been a lack of literature discussing the influence of SLA, particularly concerning sandblasting distances and acid-etching duration, on surface roughness and crystallographic aspects such as texture/crystallographic orientations and residual stress. For instance, Hung et al. (2017) performed SLA modifications on pure titanium surfaces, where sandblasting and etching were carried out with variations in sandblasting nozzle distance and etching duration on the implants. However, in their research, no investigation was conducted regarding the crystallographic aspects of the surface, such as texture and residual stress. On the other hand, Fintová et al. (2020) studied pure titanium's texture and residual stress after SLA modification. However, in their research, no parameters of the SLA process were varied.

[a]Author to whom correspondence should be addressed. Electronic mail: kris013@brin.go.id

This research aims to investigate the impact of SLA processes on pure grade IV titanium samples, focusing on surface roughness and crystallographic aspects, particularly texture and residual stress. The study considers the effects of sandblasting distances and acid-etching duration as the key parameters. Subsequently, comprehensive 3D surface roughness and X-ray diffraction (XRD) characterizations were performed on the samples.

II. EXPERIMENTAL

A. Titanium sample preparation

Grade IV pure titanium plates for dental implants with sizes $300 \times 300 \times 1$ mm were obtained from Pudak Scientific, Indonesia (Pudak Scientific, 2023). These were cut into seven $10 \times 40 \times 1$ mm plates with a MICRACUT 152 precision cutter from Metkon Instruments, Inc., Turkey (Metkon Instruments Inc., 2023a). The cutter speed settings were at 600 rpm with a cutting time of 3.15 min. The resulting plates were then mounted on a mounting made of a 1:1 mixture of locally sourced epoxy resin and an epoxy hardener component. This was done all at once, with 8 h of curing time. The mounted samples were then ground with a FORCIPOL 202 metallographic grinding and polishing machine from Metkon Instruments, Inc., Turkey (Metkon Instruments Inc., 2023b). Grit 400, 600, 800, 1000, 1500, and 2000 sandpaper were used in this process, with the grinding speed and time being 250 rpm and 5 min, respectively, for each sample. Ground samples were then polished with the same instrument by using a soft velvet cloth, a Hyprez © Five-Star © diamond compound paste from Engis Corp., USA (Engis Corp., 2023), and an OP-U NonDry colloidal silica suspension from Struers ApS, Denmark (Struers ApS, 2023). The polishing speed and time were 250 rpm and 5 min.

B. Titanium samples sandblasting and acid-etching

Grit 60 sandblasting was then applied to the prepared samples. The sandblasting was done by using a Dry Injector Sandblasting Machine Type 75 IN from Sandmaster AG, Switzerland (Sandmaster AG, 2023a). The sandblasting material used was Biloxit Bi60, made of >99.6% Al_2O_3, from Sandmaster AG, Switzerland (Sandmaster AG, 2023b). The sandblasting process was done at room temperature, i.e., at 22 to 25 °C, with the sandblaster nozzle pressure kept at 200 kPa for 60 s of sandblasting time. This constant nozzle pressure and sandblasting time were chosen to ensure a uniform surface finish on all samples. The samples were later numbered and categorized based on their variation of surface treatments. The first group of samples, i.e., samples 1–3, were sandblasted respectively at 6, 4, and 2 cm distances without a follow-on acid-etching process. The 6, 4, and 2 cm distances were taken to observe changes in the sample's characterization results incrementally. The 4 cm distance was chosen as the constant sandblasting distance for group 2 samples because it is a median value between 2 and 6 cm and thus represents a good compromise between the two extremes. Also, there is no significant difference between the sample's roughness parameters, as will be shown later. After sandblasting at a 4 cm distance, acid etching was conducted on the second group of samples (samples 4 and 5) for 30 and 60 min, respectively. This group was compared with the 4 cm sample without etching from the first group. The etching treatment uses a 1: 8: 1 mixture of HCl: H_2SO_4: H_2O and was done at room, warm, and boiling temperature conditions of 25, 75, and 105 °C, respectively. Next, Table I lists the group of samples and their sandblasting and acid-etching variations. Figures 1(a) and 1(b), respectively, illustrate the sandblasting-only and sandblasting followed by acid-etching (SLA) treatments on group 1 and group 2 samples.

C. Titanium sample characterizations

Two types of characterizations were conducted on the samples after modifying the sample surface with sandblasting and SLA. The first characterization involves assessing the surface roughness of the samples by using a confocal laser microscope. The objective was to analyze the SLA process's impact on the pure titanium surface profile. At the same time, the second characterization is an XRD analysis of texture and residual stress. This investigation aimed to explore surface modification effects from a crystallographic perspective, specifically focusing on the variations in sandblasting distance and acid-etching duration.

D. Titanium samples roughness characterizations

The sample roughness characterizations were done with a VK-X1000 3D laser scanning confocal microscope from Keyence Corp., USA (Keyence Corp., 2023). Imaging was done by using a 3D mapping method based on analytical geometry with an iridium-based laser source. Images with 50, 100, 200, 500, and 1000× magnification were taken for each sample. However, for roughness, 500× magnification was used as this allowed for large surface area imaging while still being able to observe the sample's topographic details. The surface area size for these characterizations is 338.284,9 μm². Captured images were then processed with the instrument's analytical software under a laser-differential interference contrast (DIC) processing mode. The roughness characterization involves *Sa*, *Sz*, and *Ssk* measurements with regard to the experimental parameters taken across the entire surface area. Also,

TABLE I. Summary of Grade IV titanium samples sandblasting-only and sandblasting followed by acid-etching surface treatment variations.

Sample groups	Sample No.	Sandblasting nozzle pressure (kPa)	Sandblasting duration (s)	Sample distances from sandblasting nozzle (cm)	Acid-etching duration (min)
First	1	200	60	6	N/A
	2	200	60	4	N/A
	3	200	60	2	N/A
Second	4	200	60	4	30
	5	200	60	4	60

https://doi.org/10.1017/S0885715624000320 Published online by Cambridge University Press

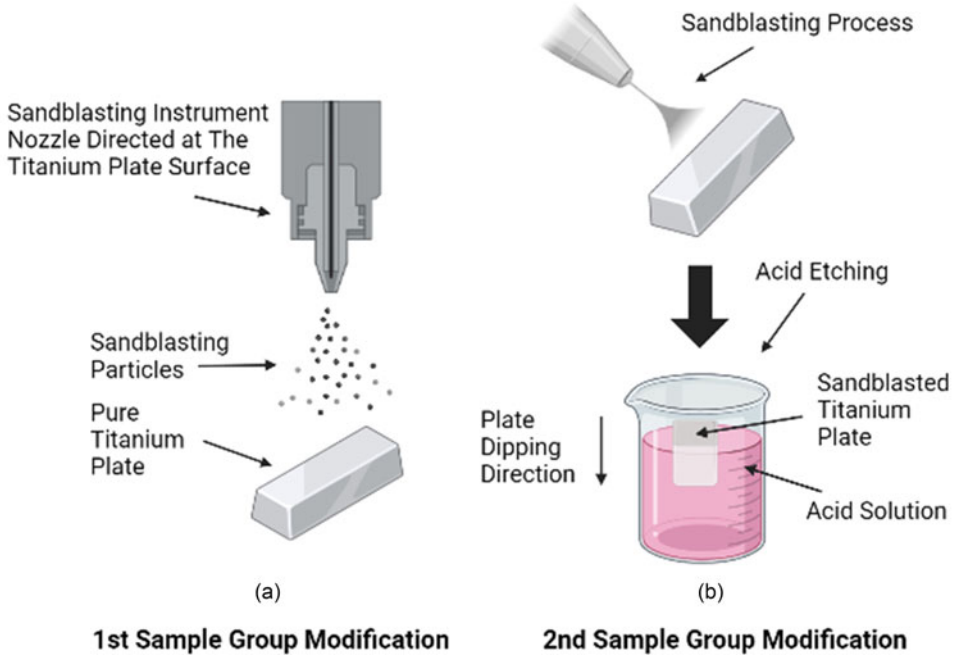

Figure 1. (Color online) Illustrations of (a) sandblasting-only treatment with biloxit Bi60 made of >99.6% Al_2O_3 on group 1 sample's surface and (b) sandblasting followed by acid-etching with a 1: 8: 1 mixture of HCl: H_2SO_4: H_2O on group 2 surface.

Straumann AG's patent provides the recommended *Sa*, *Sz*, and *Ssk* values for achieving optimal performance in titanium-based implants. This study also incorporates other types of roughness, i.e., *Sz* and *Ssk*, in order to comprehensively represent surface roughness. If $Ssk < 0$, the surface is dominated by valleys compared to peaks, and vice versa if $Ssk > 0$. Finally, the displayed 500× surface roughness visualization is referenced to *Sz* measurements since it can also serve as the sample's absolute surface height reference.

E. Titanium samples XRD characterizations

Data were obtained on a Bruker D8 Advance Eco diffractometer with Cu-$K\alpha$ beam source (1.54 Å). The source tube operates at 40 kV/25 mA, with primary and secondary soller slit of 2.5°, variable divergence slit optics setup with an illumination area of 15 mm and LYNXEYE-XET position-sensitive detector without $K\beta$ filter attached. Texture diffraction patterns are collected in the 2θ range 30°–100° step size of 0.02° and azimuth angle (φ) range 0°–90° step size of 10°. The collected texture data were processed with MAUD software by using harmonic texture with $\bar{1}$ symmetry and Popa-rules models for the microstructure (Lutterotti et al., 2004). The resulting pole plots displayed the stereographic projection of $[10\bar{1}0]$, [0002], and $[10\bar{1}3]$ orientations. The three orientations were chosen because changes in their corresponding peak intensities were the highest compared to peak changes from other orientations. As for inverse pole plots, three reference frames were used for each parameter variation, i.e., normal (ND), transverse (TD), and rolling direction (RD). The sample's ND, RD, and TD plots showed the projections of the [0001], $[10\bar{1}0]$, and $[2\bar{1}\bar{1}0]$ planes, respectively. The three planes are parallel to their respective reference frames. For pure titanium with a hexagonal close-packed (HCP) crystal structure PDF 00-044-1294 [Sailer and McCarthy (1993)], the primary slip planes are the basal [0001], prismatic $[10\bar{1}0]$, and pyramidic $[10\bar{1}1]$ planes, all with a slip direction of $[11\bar{2}0]$ relative to the planes. The resulting pole and inverse plots were compared with regard to variations in sandblasting distance and acid-etching duration.

Residual stress diffraction patterns are collected in the 2θ range 135°–145° with a step size of 0.04°, tilt angle (ψ) range −45° to +45° with a step size of 11.25°, and azimuth angle (φ) range 0° and 90°. The resulting sample strain ($\varepsilon_{\varphi\psi}^{hkl}$) from the peaks was found by first varying the sample's diffracted peak intensities (in counts) plots at $2\theta = 139°$ and ψ values of 0, 11.5, 22.5, 33.75, and 45°, and the reverse (−11.5, −22.5, etc.). The 2θ of 139° was chosen as the recommended value from the ASTM E2860-12 standard for titanium or titanium-based (ASTM International, 2023). At the same time, the previous ψ values were chosen to perform a gradual increasing and decreasing ψ scan of the sample's grain according to the instrument configuration. The collected residual stress data were then analyzed with Bruker Diffrac. Leptos software was used to evaluate the data by using sliding gravity peak evaluation and a normal + shear stress model (Bruker AXS GmbH., 2009). Residual stress determination was then repeated for each sandblasting distance parameter and etching duration. Supplementary A provides the equations used for constructing the samples pole, inverse pole, resulting strain ($\varepsilon_{\varphi\psi}^{hkl}$) vs ψ plots, as well as for residual stress determination, including its normal and shear stress components. Furthermore, the peak intensity results for group 1 and group 2 samples are also provided in the same section.

III. RESULTS AND DISCUSSION

A. Titanium samples roughness characterizations

The *Sa*, *Sz*, and *Ssk* roughness results for group 1 and group 2 samples are presented sequentially in the following manner: first, they are showcased through a 3D contour

https://doi.org/10.1017/S0885715624000320 Published online by Cambridge University Press

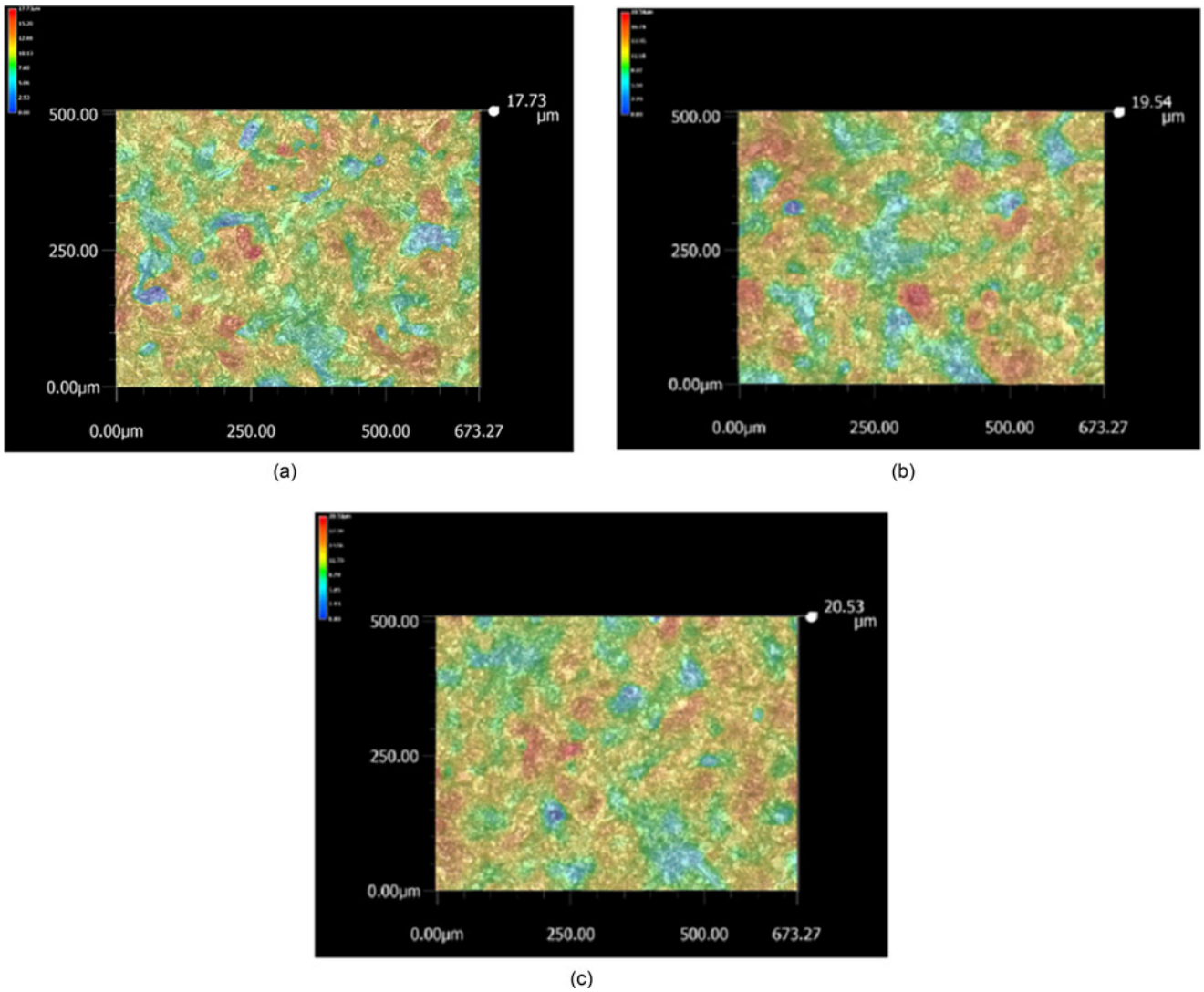

Figure 2. (Color online) 3D contour visualization of sandblasted-only samples (group 1) *Sz* roughness at sandblasting distances of (a) 6, (b) 4, and (c) 2 cm.

visualization of the *Sz* surface roughness in Figures 2(a)–2(c) and 3(a)–3(c). Then, the roughness measurement results are listed in Table II. Finally, each roughness parameter is plotted with regard to the experimental parameter variations, as seen in Figures 4(a) and 4(b).

From Figures 2(a)–2(c) results, the areas exhibiting a color gradation from green to yellow and then red represent the regions affected by sandblasting, which indicates the presence of hills and valleys distributed irregularly. The color gradation further intensifies as the features rise in elevation. These features material composition or phases are likely a mixture of sandblasting material, titanium, and other compounds present during the sandblasting process. The qualitative phases of the material are identified in the supplementary section. From Figures 3(b) and 3(c) results, it is evident that with an extended etching duration, the regions affected by both sandblasting and etching exhibit a prominent rise in hill features (indicated by the red color). This effect is particularly pronounced when contrasted with samples that underwent no etching (0 min etching), as in Figure 3(a). Furthermore, the hill features within the etched regions demonstrate a relatively uniform distribution in contrast to the areas of the sample treated solely with sandblasting.

From Table II and Figure 4(a), the group 1 sample's *Sa* and *Sz* roughness values tend to increase as the sandblasting distance is reduced. Meanwhile, *Ssk* shows a shift toward positive values and subsequently increases further as the sandblasting distance decreases. In addition, the values of *Sa*, *Sz*, and *Ssk* do not vary too significantly with sandblasting distance. Thus, the roughness results justify using a constant sandblasting distance of 4 cm for etched samples. The combined trends, along with the findings depicted in Figures 2(a)–2(c), indicate that the sample's surface is initially marked by hills interspersed with deep valleys, which subsequently transform a more hilly terrain when exposed to a sandblasting distance of 2 cm. As the sandblasting distance decreases, the sandblasting particles increasingly envelop the remaining valleys, ultimately creating the rugged features observed on the surface. The trend observed in Table II and Figure 4(a), along with the findings depicted in Figures 2(a)–2(c), aligns with earlier findings documented in existing literature (Jiang et al., 2006; Iwaya et al., 2008; Pazos et al., 2010; Sadrkhah et al., 2023).

From Table II and Figure 4(b), group 2 *Sa* and *Sz* roughness values indicate a trend of decreasing roughness as the etching duration increases from 0 to 30 and then to 60 min.

https://doi.org/10.1017/S0885715624000320 Published online by Cambridge University Press

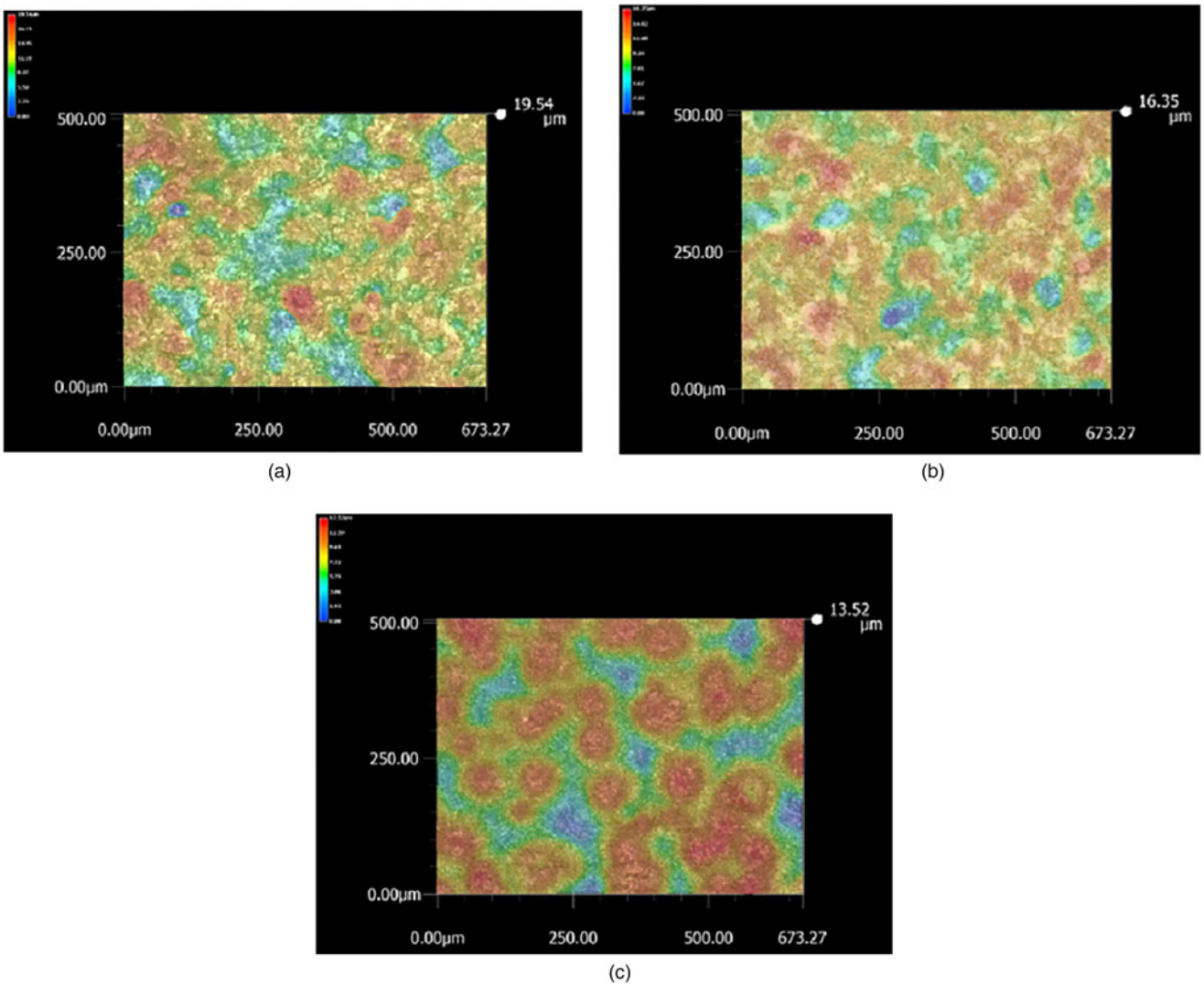

Figure 3. (Color online) 3D contour visualization of 4 cm sandblasted followed by acid-etched samples (group 2) *Sz* roughness at (a) 0, (b) 30, and (c) 60 min etching durations.

TABLE II. Summary of sandblasted-only (group 1) and sandblasted followed by acid-etching (group 2) samples *Sa*, *Sz*, and *Ssk* results.

Sample groups	Sample No.	Sample distances from sandblasting nozzle (cm)	Acid-etching duration (min)	*Sa*	*Sz*	*Ssk*
First	1	6	N/A	1.49 ± 0.02	17.74 ± 0.96	−0.43 ± 0.01
	2	4	N/A	1.82 ± 0.02	19.54 ± 1.31	−0.03 ± 0.01
	3	2	N/A	1.59 ± 0.01	20.53 ± 1.61	−0.14 ± 0.04
Second	4	4	30	1.35 ± 0.01	16.36 ± 1.24	−0.44 ± 0.01
	5	4	60	1.19 ± 0.01	13.76 ± 0.70	−0.60 ± 0.04

These include the sample's sandblasting and acid-etching treatment variations.

Meanwhile, *Ssk* experiences a shift toward a more negative value as the etching duration increases. The trends of *Sa*, *Sz*, and *Ssk* indicate that hills and valleys predominantly characterize the initial surface characteristics of the sample. However, as the etching process duration increases, these characteristics undergo a notable shift, leading to a marked elevation in hill features and a simultaneous emergence of more profound valleys. Regarding Figures 3(a) and 3(b), the reduced area due to etching is also accompanied by a decrease in roughness. These trends align with findings reported in the literature (Kim et al., 2008). Finally, sample number 5, with an etching duration of 60 min, shows *Sa*, *Sz*, and *Ssk* values that closely approximate the *Sa*, *Sz*, and *Ssk* values outlined in the Straumann patent previously.

B. Titanium samples crystallographic texture measurements with XRD

The crystallographic texture characterization results for both group 1 and group 2 surfaces, including the slip plane and reference direction parallel to the texture orientation, are presented in the form of 3D structures in HCP pole and inverse

https://doi.org/10.1017/S0885715624000320 Published online by Cambridge University Press

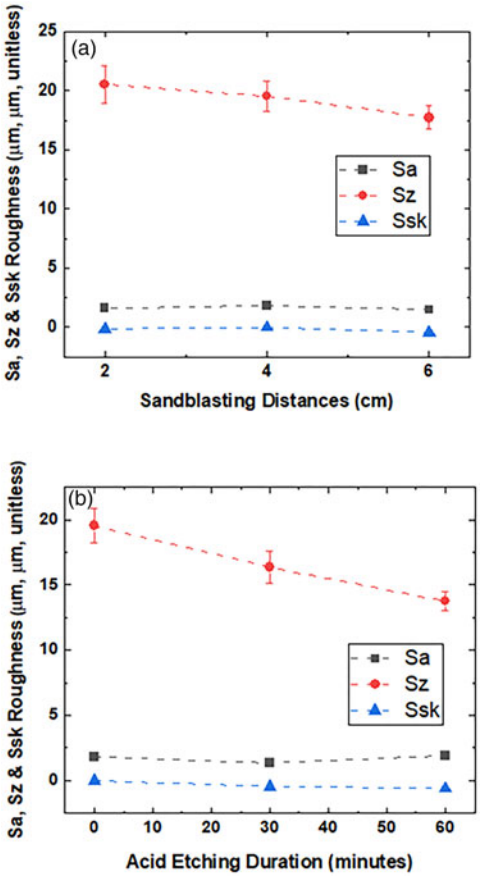

Figure 4. (Color online) The *Sa* (black square), *Sz* (red circle), and *Ssk* (blue triangle) roughness plot of (a) group 1 samples (sandblasting-only) with respect to sandblasting distances of 6, 4, and 2 cm, and (b) group 2 samples (sandblasting followed by etching) with respect to 0, 30, and 60 min etching durations, at a sandblasting distance of 4 cm.

pole figures in Figures 5(a)–5(d) and 6(a)–6(c). Both groups' plots varied with regard to the experimental parameters.

From Figure 5(b) pole plot, it is evident that the $[10\bar{1}0]$, [0002], and $[10\bar{1}3]$ orientations of group 1 are either positioned parallel or at certain angles with respect to the sandblasting direction. Here, the most significant orientation intensities were the middle red [0002] and orange $[10\bar{1}3]$ contours which show intensities of approximately ∼1.4 and 1.2 mrd, respectively. Hence, both planes are significantly impacted by sandblasting, with the $[10\bar{1}3]$ intensity being lower than [0002] due to its non-parallel position with respect to the (sandblasting) spray direction. The orientations identified in Supplementary B of the supplementary section correspond to the presence of titanium and corundum (Al_2O_3) PDF 00-046-1212 [Huang et al. (1989)] compounds. This observation is further corroborated by the inverse pole plot in Figure 5(b), where the ND central contour (in red) and the TD edge contour (in yellow) indicate high orientation intensities of approximately ∼1.2 and 1.1 mrd, respectively. Here, since $[10\bar{1}3]$ is at a specific angle with respect to $[2\bar{1}\bar{1}0]$ in TD, the intensity of $[10\bar{1}3]$ can still be observed, although smaller than [0002].

Furthermore, because [0002] is parallel to the [0001] slip plane, sandblasting will create hills in the [0002] orientation. This occurs as atoms in the orientation undergo shifts in the $[1\bar{1}20]$ direction. The same phenomenon is also observed at the $[10\bar{1}3]$ orientation; however, the hills created in this orientation are smaller than those in the [0002] orientation. In addition, although $[10\bar{1}0]$ is its own slip plane, the hills created here are even less significant compared to those in [0002] and $[10\bar{1}3]$. This is due to reduced sandblasting impact in $[10\bar{1}0]$ compared to [0002] and $[10\bar{1}3]$, since $[10\bar{1}0]$ is likely normal with respect to the sandblasting direction. Hence, the orientation intensities in Figures 5(b)–5(d) correspond to the increased hill intensities (marked by red and orange colors) that are present during the sandblasting procedure.

As the sandblasting distance decreases, the dominant hill intensities in the [0002] and $[10\bar{1}3]$ planes [Figures 5(b)–5(d)] become more pronounced. This transition is highlighted by the consistent [0002] and $[10\bar{1}3]$ orientation intensities and color depicted in Figures 5(b)–5(d), accompanied by an increase in the hill intensities of $[10\bar{1}0]$ planes, as the sandblasting distance decreases. This can be seen in the red part of [0001] ND and the yellow edge of $[2\bar{1}\bar{1}0]$ TD inverse pole plot. While for $[10\bar{1}0]$, the transformation is evident in the cyan part of $[10\bar{1}0]$ RD inverse pole plot that changes into a near-yellow hue as the sandblasting distance decreases. Thus, as the sandblasting distance decreases, the sandblasting process begins to impact orientations perpendicular to the sandblasting direction. Also, decreasing sandblasting distance likely correlates with an increased presence of corundum compounds from the material due to stronger hill intensities observed in the [0002] and $[10\bar{1}3]$ planes. In terms of roughness characterization results, group 1 samples show increased hill intensities with decreasing sandblasting distance due to atomic shifts in impacted orientations.

From group 2 texture results, the sample's pole and inverse pole plots with 0 min etching duration and sandblasting distance of 4 cm [Figure 6(a)] serve as a reference texture for group 2 analysis. For a 30 min-etched sample [Figure 6(b)], it can be seen that the impacted area has shifted to other planes positioned at certain angles with respect to the [0002] orientation. In addition, the impacted area is not parallel to $[10\bar{1}3]$, where the area itself appears to be significantly reduced. This is evident from the change of color in the [0002] plane central contour to dark blue and the reduction in $[10\bar{1}3]$ intensity, with the plane's intensities becoming ∼0.8 and ∼1.1 mrd, respectively. Also, sandblasting with etching appears to have affected the $[10\bar{1}0]$ plane, as shown by the shift in its central contour color from dark blue to yellow. Moreover, the $[10\bar{1}0]$ plane intensities experienced an increase from ∼0.8 to ∼1.1 mrd. These changes are particularly evident when compared to the Figure 6(a) sample. The impact of sandblasting with etching is further corroborated in the inverse pole plot of Figure 6(b), showing changes in color and a decrease in orientation intensity in the ND and RD central contour, as well as in the TD plot's edge. The ND plot also suggests a shift in the impacted area from the [0002] to the $[\bar{1}120]$ family of planes, encompassing $[\bar{1}\bar{1}20]$, $[1\bar{1}20]$, and [1120] planes.

For a 60 min-etched sample [Figure 6(c)], the impacted area is seen to extend from the [0002] plane central contour to other planes positioned at certain angles with respect to [0002]. This is due to a notable increase in orientation intensities at both positions, reaching 2.5 to 3.5 mrd, with a change in color to an orange hue. Meanwhile, the $[10\bar{1}0]$ orientation undergoes further reduction during the etching process, indicated by the shift in the plane's middle contour color from yellow to dark blue, along with a decrease in intensity from ∼1.1

https://doi.org/10.1017/S0885715624000320 Published online by Cambridge University Press

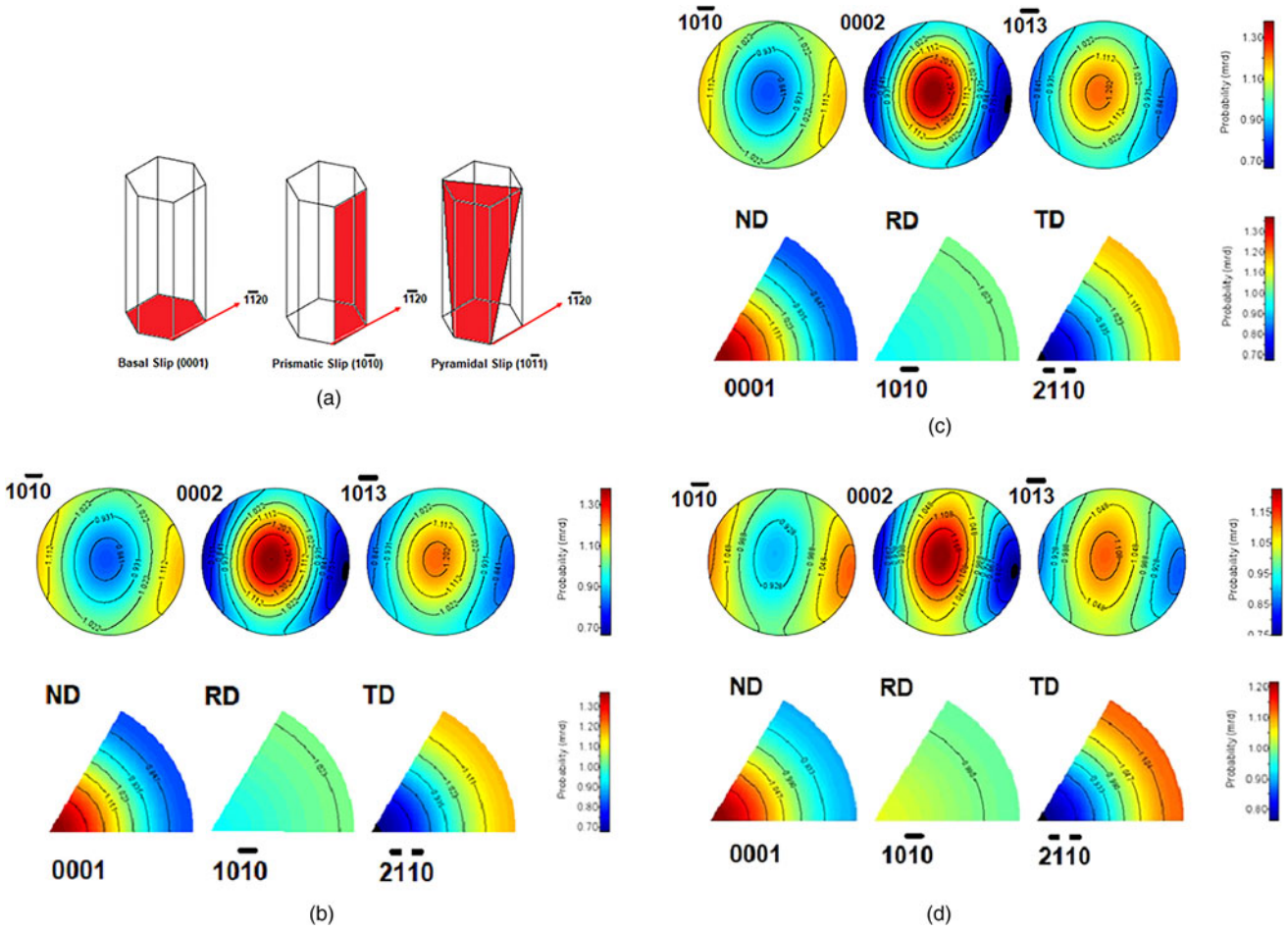

Figure 5. (Color online) (a) illustrations of the basal [0001], prismatic [10$\bar{1}$0], and pyramidic [10$\bar{1}$1] slip planes with the corresponding slip direction [1$\bar{1}$20] parallel to the planes. The pole (top circle) and inverse pole (bottom triangle) plots are depicted for sandblasted-only (group 1) samples at sandblasting distances of (b) 6, (c) 4, and (d) 2 cm. The pole's orientation plane is [10$\bar{1}$0], [0002], and [10$\bar{1}$3], respectively. Meanwhile, the inverse pole plots reference frame consists of the normal (ND), transverse (TD), and rolling directions (RD), which are parallel to the [0001], [10$\bar{1}$0], and [2$\bar{1}$$\bar{1}$0] projections, respectively.

to ~0.5 mrd. In addition, the impacted area is relatively parallel to the [10$\bar{1}$3] plane. Hence, there is an increase in intensity to 3.5 mrd and a color change to red compared to the previous etching duration. The effect of prolonged etching duration is evident in Figure 6(c) inverse pole plot. The ND central contour shows a color change and a similar intensity increase seen in the sample's pole plot. On the other hand, the RD and TD edge contour experience a color change to light blue, accompanied by a decrease in intensity values to 1.5 mrd. Note that with extended etching duration, the impacted area elongation in [0002] will influence the [$\bar{1}$120] family of planes as in the previous duration, with the impacted area having shifted or no longer present in the TD.

To conclude, in Figure 6(b), after sandblasting and a 30-min etching process, the etching solution will first reduce the hill and valley features parallel to the [0002] plane and then shift the impacted area to the [$\bar{1}$120] family of planes. Meanwhile, sandblasting with etching will also reduce the hill features in [10$\bar{1}$0] plane. The [10$\bar{1}$0] slip system serves as its own slip plane, and hill feature reduction occurs by way of atomic shift within this system. In addition, etching will also reduce the hill and valley features in the [10$\bar{1}$3] plane and the impacted area is on the verge of shifting to other orientations. From Figure 6(c), when the etching duration is further increased, the etching solution enhances the hill features while simultaneously giving rise to deep valley characteristics, aligning in parallel with [0002] and [$\bar{1}$120] orientations. The increased etching duration similarly applies to the hill enhancement process that occurred on the [0002] and the [10$\bar{1}$3] planes. These results can be used to explain the surface roughness trends and features of group 2 samples. At an etching duration of 0 min and a sandblasting distance of 4 cm, the corundum compound is still present, as evidenced by stronger hill intensities observed in the [0002] and [10$\bar{1}$3] planes. However, these intensities decrease significantly with longer etching durations. Conversely, a new phase, titanium hydride (TiH_2) PDF 01-080-2507 [Kalita et al. (2010)] gradually appears, correlating with the shift in dominant orientation from the [0002] plane to the [$\bar{1}$120] plane. Overall, group 1 and 2 pole and inverse pole plot characteristics have been reported in previous literature (Fintová et al., 2020). The surface feature reduction process in Figures 6(a)–6(c) with varying etching durations also aligns with the findings reported in previous literature (Yi et al., 2022).

C. Titanium samples residual stress from XRD characterizations

The residual stress characterization results for group 1 and 2 samples are displayed in Figures 7 and 8 as plots of $\varepsilon_{\varphi\psi}^{hkl}$ vs

https://doi.org/10.1017/S0885715624000320 Published online by Cambridge University Press

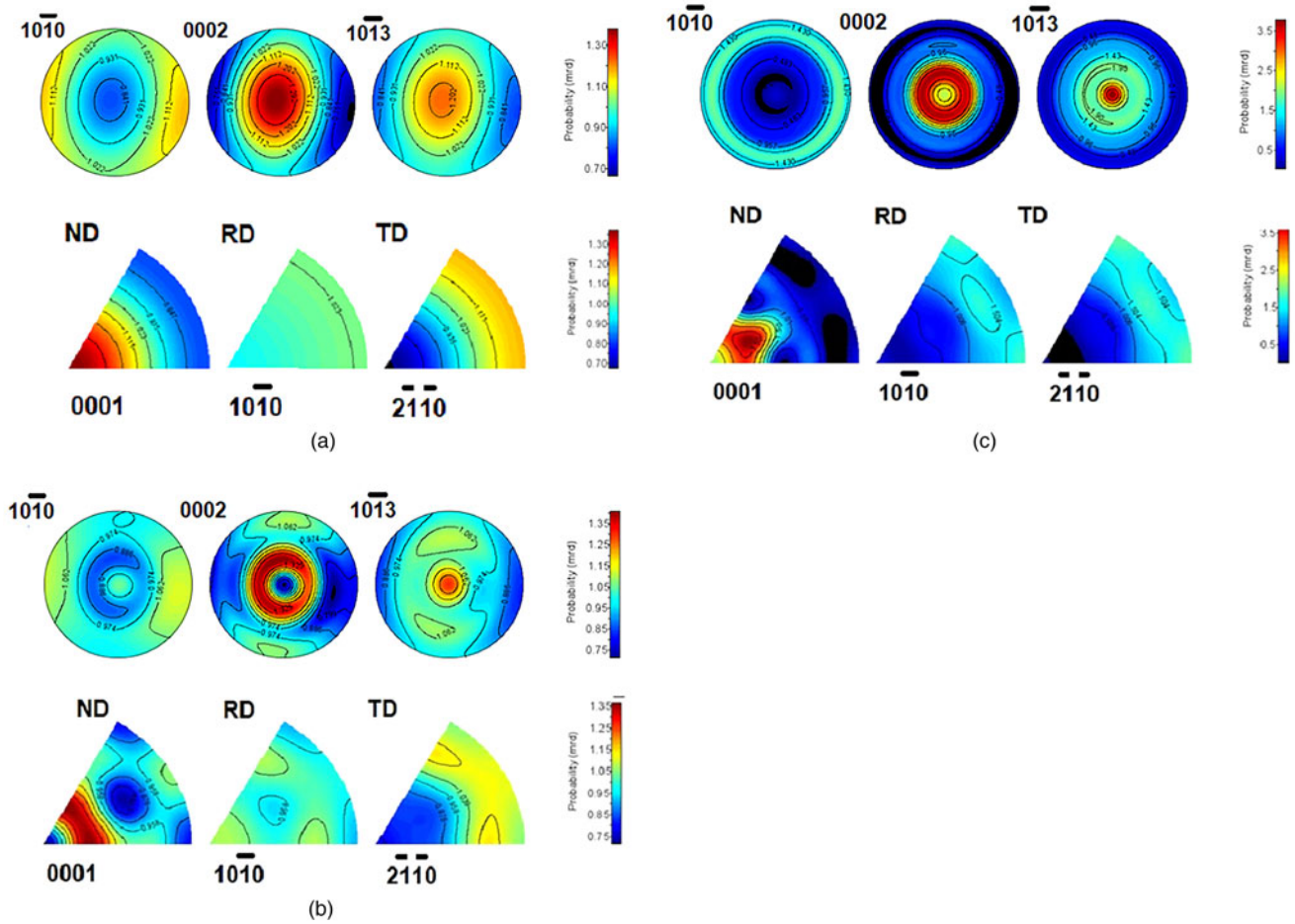

Figure 6. (Color online) The pole (top circle) and inverse pole plot (bottom triangle) of sandblasted followed by etched samples (group 2) with respect to (a) 0, (b) 30, and (c) 60 min sandblasting duration at a sandblasting distance of 4 cm. The slip planes, orientation poles, reference frames, and projected planes in group 2 are the same as those in Figures 5(a)–5(d). Orientation shifts in (b) and (c) likely occur from [0002] in (a) to the [$\bar{1}$. 120] family of planes. Here, Figure 5(b) results from group 1 serve as a comparison to the texture outcomes of group 2 samples.

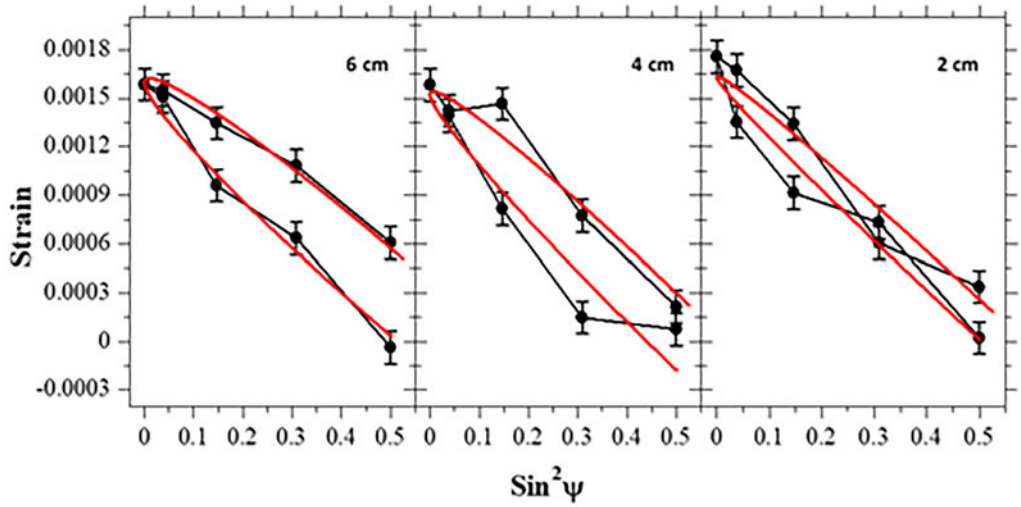

Figure 7. (Color online) XRD results of $\varepsilon_{\varphi\psi}^{hkl}$ strain vs $\sin^2\psi$ plots: sandblasted-only or first sample group plots (in black) with respect to decreasing sandblasting distances at (left) 6, (center) 4, and (right) 2 cm. The red plots are the black plot's fitting curve.

$\sin^2\psi$, with regard to the experimental parameters variations. From each plot, the sample's normal and shear stress values were then obtained and presented in Tables III and IV, together with the related experimental parameters variations.

From Figure 7, the measured strain on the sample's surface is inversely proportional to the plot's ψ angle. As the resulting strain increases, the angle ψ used in the plot equation also decreases. From the measured strain, the stress applied to

https://doi.org/10.1017/S0885715624000320 Published online by Cambridge University Press

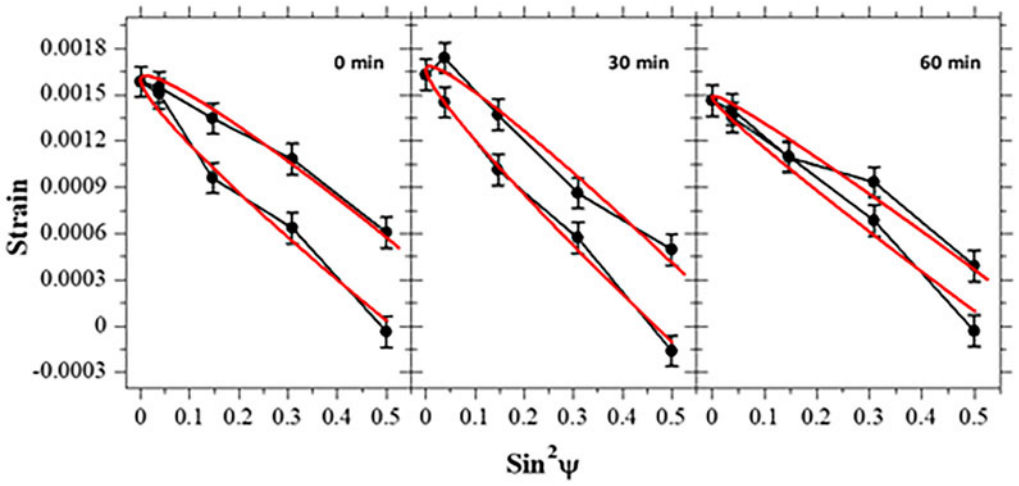

Figure 8. (Color online) XRD results of $\varepsilon_{\varphi\psi}^{hkl}$ strain vs $\sin^2\psi$ plots: sandblasted with acid etched or second sample group plots (in black) with respect to increased acid-etching duration from (left) 0, (center) 30, and (right) 60 min, at a constant sandblasting distance of 4 cm. The red plots are again the black plot's fitting curve.

TABLE III. Summary of the residual stresses in the sandblasted-only or first sample group normal and shear stress (in MPa) at a sandblasting distance of 6, 4, and 2 cm

Samples	Sample distances from sandblasting nozzle (cm)	Acid-etching duration (min)	Normal stress (MPa)	Shear stress (MPa)
1	6	N/A	−220.9 ± 12.6	23.1 ± 3.1
2	4	N/A	−250.1 ± 29.2	20.4 ± 7.1
3	2	N/A	−268.5 ± 16.7	14.6 ± 4.1

Note that normal stress, being applied to the sample, is represented as a negative (−) value, while shear stress is depicted as positive (+) since it acts in the opposite direction compared to compressive stress.

TABLE IV. Summary of the second sample group normal and shear stress (in MPa) with respect to increased acid-etching duration from 0, 30 to 60 min at a constant sandblasting distance of 4 cm

Samples	Sample distances from sandblasting nozzle (cm)	Acid-etching duration (min)	Normal stress (MPa)	Shear stress (MPa)
2	4	0	−250.1 ± 29.2	20.4 ± 7.1
4	4	30	−258.4 ± 12.7	22.1 ± 3.1
5	4	60	−214.6 ± 15.5	11.4 ± 3.8

Note again that normal stress is stated as a (−) value, while shear stress is expressed as a (+) value.

the surface (not shown in Figure 7) will be directly proportional to ψ in the plot's equation. This relationship between strain and stress vs ψ applies to all variations of sandblasting distances. It can also be seen in the plot that as the sandblasting distance decreases, the normal stress component dominates the residual stress on the surface of the group 1 sample. This occurs because the relationship between $\varepsilon_{\varphi\psi}^{hkl}$ vs $\sin^2\psi$ in the plot becomes relatively linear at smaller sandblasting distances. This is further confirmed by the normal and shear stress values in Table III, where the normal stress is significantly larger than the shear stress. In addition, with a decrease in the sandblasting distance, the significant difference between the normal and shear stress values grows larger. These results align with the changes in residual stress observed in previous literature (Osak et al., 2021). Also, as the sandblasting distance decreases, the shear stress decreases as well. This is likely due to the tendency of the sandblasting direction to be normal, rather than parallel, to the sample's surface. With regard to the sample's surface roughness and texture results, the normal stress component of the residual stress induces the formation of hills, which are then enhanced as the sandblasting distance decreases.

From Figure 8, it can be seen that the plot features remain consistent with those in Figure 7. This is also evident from the normal and shear stress values in Table IV. The normal stress value greatly surpasses the shear stress value, and the difference between normal and shear stress values slightly increases from 0 to 30 min. At 60 min of etching, both normal and shear stresses decrease, but the normal stress remains larger than the shear stress. Therefore, Figure 8 plot exhibits a relatively linear trend as the etching duration increases, driven by the predominance of normal stress over shear stress values. From Figure 8 and Table IV, as the etching duration increases, the sandblasting with the etching process will reduce the normal stress component on the group 2 sample's surface. The normal stress component of the residual stress decreasing trend aligns with the initial reduction in hill and valley features within the samples, and subsequent hill enhancement at extended etching duration. This is consistent with residual stress changes in previous literature with regards to etching duration (Pazos et al., 2010). In addition, the shear stress component of the sample decreases as the etching duration lengthens. This can be attributed to the previous hill enhancement processes.

IV. CONCLUSION

This study addresses the influence of sandblasted, large-grit, acid-etched (SLA) modification on the surface characteristics of pure grade IV titanium, commonly used in dental and

https://doi.org/10.1017/S0885715624000320 Published online by Cambridge University Press

bone implants. Enhanced surface roughness is vital for implant performance, and SLA offers a promising approach by creating an optimum rough surface. The investigation uniquely considers the joint impact of sandblasting distances and acid-etching duration on surface roughness and crystallographic features. Conducting comprehensive 3D surface roughness and XRD characterizations bridges the gap in prior research by examining modification parameters and crystallographic aspects. Crystallographic texture analysis indicated that sandblasting influenced slip planes, which affected orientation intensities. Combined with etching, varied roughness, and texture outcomes are produced based on the etching duration. The residual stress analysis supported these findings, showing the dominance of surface modification. The results contribute to a comprehensive understanding of these techniques for titanium applications on implant surfaces, offering potential advances in implantology techniques.

SUPPLEMENTARY MATERIAL

The supplementary material for this article can be found at https://doi.org/10.1017/S0885715624000320.

ACKNOWLEDGEMENTS

The authors wish to thank Pudak Scientific, Indonesia, for their kind assistance and support in the preparation of the titanium samples used in this article. The authors acknowledge the facilities, scientific and technical support from Advanced Characterization Laboratories Serpong, National Research and Innovation Agency through E-Layanan Sains, Badan Riset dan Inovasi Nasional.

CONFLICTS OF INTEREST

The authors declare that they have no known competing financial interests or personal relationships that could have appeared to influence the work reported in this paper.

REFERENCES

ASTM International 2023. Standard Test Method for Residual Stress Measurement by X-Ray Diffraction for Bearing Steels. Accessed March 10, 2023. https://www.astm.org/e2860-12.html

Berner, S. 2016. Process for the Preparation of a Topography for Improved Protein Adherence on a Body made of Titanium or a Titanium Alloy. WIPO Patent WO2016189099A1, filed May 26, 2016, and issued December 1, 2016.

Bruker AXS GmbH. 2009. DIFFRAC.LEPTOS. Accessed March 10, 2023. https://www.bruker.com/de/products-and-solutions/diffractometers-and-x-ray-microscopes/x-ray-diffractometers/diffrac-suite-software/diffrac-leptos.html

Buser, D., R. K. Schenk, S. Steinemann, J. P. Fiorellini, C. H. Fox, and H. Stich. 1991. "Influence of Surface Characteristics on Bone Integration of Titanium Implants. A Histomorphometric Study in Miniature Pigs." *Journal of Biomedical Materials Research* 25 (7): 889–902. doi:10.1002/jbm.820250708.

Carlsson, L., T. Röstlund, B. Albrektsson, T. Albrektsson, and P. I. Brånemark. 1986. "Osseointegration of Titanium Implants." *Acta Orthopaedica Scandinavica* 57 (4): 285–89. doi:10.3109/17453678608994393.

Donley, T. G., and W. B. Gillette. 1991. "Titanium Endosseous Implant-Soft Tissue Interface: A Literature Review." *Journal of Periodontology* 62 (2): 153–60. doi:10.1902/jop.1991.62.2.153.

Engis Corp. 2023. Hyprez® Diamond Compound. Accessed March 2, 2023. https://www.engis.com/hyprez-diamond-compound

Fintová, S., I. Kuběna, J. Palán, K. Mertová, M. Duchek, P. Hutař, F. Pastorek, and L. Kunz. 2020. "Influence of Sandblasting and Acid Etching on Fatigue Properties of Ultra-Fine Grained Ti Grade 4 for Dental Implants." *Journal of the Mechanical Behavior of Biomedical Materials* 111: 104016. doi:10.1016/j.jmbbm.2020.104016.

Huang, T. C., W. Parrish, N. Masciocchi, and P. W. Wang. 1989. "Derivation of d-Values from Digitized X-ray and Synchrotron Diffraction Data." *Advances in X-ray Analysis* 33: 295–303. doi:10.1154/S0376030800019698.

Hung, K. Y., Y. C. Lin, and H. P. Feng. 2017. "The Effects of Acid Etching on the Nanomorphological Surface Characteristics and Activation Energy of Titanium Medical Materials." *Materials* 10 (10): 1164. doi:10.3390/ma10101164.

Iwaya, Y., M. Machigashira, K. Kanbara, M. Miyamoto, K. Noguchi, Y. Izumi, and S. Ban. 2008. "Surface Properties and Biocompatibility of Acid-Etched Titanium." *Dental Materials Journal* 27 (3): 415–21. doi:10.4012/dmj.27.415.

Jiang, X. P., X. Y. Wang, J. X. Li, D. Y. Li, C. S. Man, M. J. Shepard, and T. Zhai. 2006. "Enhancement of Fatigue and Corrosion Properties of Pure Ti by Sandblasting." *Materials Science and Engineering: A* 429 (1-2): 30–5. doi:10.1016/j.msea.2006.04.024.

Kalita, P. E., S. V. Sinogeikin, K. Lipinska-Kalita, T. Hartmann, X. Ke, C. Chen, and A. Cornelius. 2020. "Equation of State of TiH_2 up to 90 GPa: A Synchrotron X-ray Diffraction Study and Ab Initio Calculations." *Journal of Applied Physics* 108 (4): 043511. doi:10.1063/1.3455858.

Keyence Corp. 2023. 3D Laser Scanning Microscope – VK-X1000. Accessed March 3, 2023. https://www.keyence.com/landing/lpc/laser-microscope-gss.jsp

Kim, H., S. H. Choi, J. J. Ryu, S. Y. Koh, J. H. Park, and I. S. Lee. 2008. "The Biocompatibility of SLA-Treated Titanium Implants." *Biomedical Materials* 3 (2): 025011. 10.1088/1748-6041/3/2/025011.

Klokkevold, P. R., R. D. Nishimura, M. Adachi, and A. Caputo. 1997. "Osseointegration Enhanced by Chemical Etching of the Titanium Surface. A Torque Removal Study in the Rabbit." *Clinical Oral Implants Research* 8 (6): 442–47. doi:10.1034/j.1600-0501.1997.080601.x.

Lutterotti, L., D. Chateigner, S. Ferrari, and J. Ricote. 2004. "Texture, Residual Stress and Structural Analysis of Thin Films Using A Combined X-ray Analysis." *Thin Solid Films* 450 (1): 34–41. doi:10.1016/j.tsf.2003.10.150.

Medvedev, A. E., A. Molotnikov, R. Lapovok, R. Zeller, S. Berner, P. Habersetzer, and F. D. Torre. 2016. "Microstructure and Mechanical Properties of Ti–15Zr Alloy Used as Dental Implant Material." *Journal of the Mechanical Behavior of Biomedical Materials* 62: 384–98. doi:10.1016/j.jmbbm.2016.05.008.

Metkon Instruments Inc. 2023a. MICRACUT 152. Accessed March 2, 2023. https://www.metkon.com/mobile/en/products-details/1/132/35/micracut-152

Metkon Instruments Inc. 2023b. FORCIPOL 202. Accessed March 2, 2023. https://www.metkon.com/mobile/Products-Details/3/146/21/FORCIPOL%20202/

Monetta, T., and F. Bellucci. 2012. "The Effect of Sand-blasting and Hydrofluoric Acid Etching on Ti CP 2 and Ti CP 4 Surface Topography." *Open Journal of Regenerative Medicine* 1 (3): 41–50. doi:10.4236/ojrm.2012.13007.

Osak, P., J. Maszybrocka, M. Zubko, J. Rak, S. Bogunia, and B. Łosiewicz. 2021. "Influence of Sandblasting Process on Tribological Properties of Titanium Grade 4 in Artificial Saliva for Dentistry Applications." *Materials* 14 (24): 7536. doi:10.3390/ma14247536.

Pazos, L., P. Corengia, and H. Svoboda. 2010. "Effect of Surface Treatments on the Fatigue Life of Titanium for Biomedical Applications." *Journal of The Mechanical Behavior of Biomedical Materials* 3 (6): 416–24. doi:10.1016/j.jmbbm.2010.03.006.

Pudak Scientific. 2023. Products. Accessed March 2, 2023. https://www.pudak-scientific.com/products.php

Sadrkhah, M., G. Faraji, S. Khorasani, and M. Mesbah. 2023. "Excellent Mechanical Properties, Wettability and Biological Response of Ultrafine-Grained Pure Ti Dental Implant Surface Modified by SLActive." *Journal of Materials Engineering and Performance* 32 (24): 11408–21. doi:10.1007/s11665-023-07928-z.

Sailer, R., and G. McCarthy. 1993. *ICDD Grant-in-Aid 1993*. Fargo, ND, USA, JCPDS Database, North Dakota State University.
Sandmaster AG. 2023a. Injector Blasting Unit 75 IN. Accessed March 3, 2023. https://www.sandmaster-technology.com/EN/sandblasting-units-detail/75-in-/18
Sandmaster AG. 2023b. Sandblasting Media. Accessed March 3, 2023. https://www.sandmaster- technology.com/EN/sandblasting-media
Semlitsch, M. 1987. "Titanium Alloys for Hip Joint Replacements." *Clinical Materials* 2 (1): 1–13. doi:10.1016/0267-6605(87)90015-1.
Struers, S. A. S. 2023. Metallographic Oxide Polishing Suspensions. Accessed March 2, 2023. https://www.struers.com/en/Products/Grinding-and-Polishing/Grinding-and-polishing-consumables/Oxide-Polishing.
Wennerberg, A., and T. Albrektsson. 2009. "Effects of Titanium Surface Topography on Bone Integration: A Systematic Review." *Clinical Oral Implants Research* 20 (s4): 172–84. doi:10.1111/j.1600-0501.2009.01775.x.
Yi, X., A. Ma, L. Zhang, and Y. Zheng. 2022. "Crystallographic Anisotropy of Corrosion Rate and Surface Faceting of Polycrystalline 90Cu-10Ni in Acidic NaCl Solution." *Materials & Design* 215: 110429. doi:10.1016/j.matdes.2022.110429.

https://doi.org/10.1017/S0885715624000320 Published online by Cambridge University Press